High-Resolution Tissue Mass Spectrometry Imaging Reveals a Refined Functional Anatomy of the Human Adult Adrenal Gland

Na Sun,[1] Yin Wu,[1] Kazutaka Nanba,[2] Silviu Sbiera,[3] Stefan Kircher,[4] Thomas Kunzke,[1] Michaela Aichler,[1] Sabina Berezowska,[5] Joachim Reibetanz,[6] William E. Rainey,[2] Martin Fassnacht,[3,7,8] Axel Walch,[1] and Matthias Kroiss[3,7,8]

[1]Research Unit Analytical Pathology, Helmholtz Zentrum München, German Research Center for Environmental Health (GmbH), 85764 Neuherberg, Germany; [2]Department of Molecular and Integrative Physiology, University of Michigan, Ann Arbor, Michigan 48109-5622; [3]Department of Internal Medicine, Division of Endocrinology and Diabetology, University Hospital Würzburg, University of Würzburg, 97080 Würzburg, Germany; [4]Institut für Pathologie, University of Würzburg, 97080 Würzburg, Germany; [5]Institut für Pathologie, Universität Bern, 3008 Bern, Switzerland; [6]Department of General, Visceral, Vascular and Paediatric Surgery, University Hospital Würzburg, 97080 Würzburg, Germany; [7]Comprehensive Cancer Center Mainfranken, University of Würzburg, 97080 Würzburg, Germany; and [8]Clinical Chemistry and Laboratory Medicine, University Hospital Würzburg, 97080 Würzburg, Germany

In the adrenal gland, neuroendocrine cells that synthesize catecholamines and epithelial cells that produce steroid hormones are united beneath a common organ capsule to function as a single stress-responsive organ. The functional anatomy of the steroid hormone–producing adrenal cortex and the catecholamine-producing medulla is ill defined at the level of small molecules. Here, we report a comprehensive high-resolution mass spectrometry imaging (MSI) map of the normal human adrenal gland. A large variety of biomolecules was accessible by matrix-assisted laser desorption/ionization–Fourier transform–ion cyclotron resonance MSI, including nucleoside phosphates indicative of oxidative phosphorylation, sterol and steroid metabolites, intermediates of glycolysis and the tricarboxylic acid cycle, lipids, and fatty acids. Statistical clustering analyses yielded a molecularly defined adrenal anatomy of 10 distinct molecular zones including a highly structured corticomedullary interface. By incorporating pathway information, activities of carbohydrate, amino acid, and lipid metabolism as well as endocrine bioactivity were revealed to be highly spatially organized, which could be visualized as different molecularly defined zones. Together, these findings provide a molecular definition of human adult adrenal gland structure beyond classical histological anatomy. (***Endocrinology*** **159: 1511–1524, 2018)**

The bilateral symmetrical adrenal glands, located above the cranial poles of the kidneys within the retroperitoneal space, are the source of two major types of hormones: steroids and catecholamines. Through the action of these hormones, the adrenal glands regulate metabolic, cardiovascular, immune, neuronal, and mental processes in response to exogenous stress and other stimuli. They are key regulators for coping with salt balance, critical illness, and systemic inflammation that is enabled through the unique combination of two morphologically and developmentally distinct organs beneath a common organ capsule. Whereas the catecholamine-producing adrenal medulla is embryonically of neuroectodermal origin, the steroid hormone–producing adrenocortical cells derive from the adrenogonadal primordium descending from the coelomic wall (1). The adrenal cortex of the adult

ISSN Online 1945-7170

Received 16 January 2018. Accepted 22 January 2018.
First Published Online 29 January 2018

Abbreviations: ADP, adenosine 5′-diphosphate; ATP, adenosine triphosphate; DAN, transplantation donor adrenal; DHEA-S, dehydroepiandrosterone sulfate; FFPE, formalin-fixed paraffin-embedded; H&E, hematoxylin and eosin; IHC, immunohistochemistry; MALDI-FT-ICR, matrix-assisted laser desorption/ionization–Fourier transform–ion cyclotron resonance; MS/MS, tandem mass spectrometry; MSI, mass spectrometry imaging; RRID, Research Resource Identifier; TCA, tricarboxylic acid; UDP, uridine diphosphate; ZF, zona fasciculata; ZG, zona glomerulosa; ZR, zona reticularis.

human is classically divided into three subzones, namely, the zona glomerulosa (ZG), zona fasciculata (ZF), and zona reticularis (ZR). Each zone has a characteristic histology and primarily secretes different types of steroid hormones (2–4). The ZG is the origin of mineralocorticoids, which play an important role in salt and water regulation, relating to blood pressure and electrolyte balance (5). The ZF produces glucocorticoids, which are regulated within a feedback loop of the hypothalamic-pituitary-adrenal axis. They are strongly involved in immune response and metabolism (6). The ZR is the source of androgens and precursor hormones and develops during postnatal life (7). At variance, the adrenal medulla produces epinephrine and norepinephrine, which fulfill functions as part of the sympathetic nervous system and provide rapid responses to stress (2). As a whole, the adrenal glands play a multifaceted and critical role in the endocrine system by regulating and maintaining mineral balance, glucose metabolism, and early sexual differentiation (1). The preeminent role of the adrenal gland is illustrated through the severe consequences of adrenal dysfunction as in Addison disease (8, 9) or glucocorticoid excess resulting in Cushing syndrome (10), but also in genetic conditions such as congenital adrenal hyperplasia, which results from inactivating mutations in steroidogenic enzymes (11). Neoplasms of the adrenal gland involve frequent adrenocortical adenomas and rare diseases including adrenocortical carcinoma (12) and pheochromocytoma (13). During the past few years, tremendous progress has been made in elucidating the genetic alterations that cause development of both benign (14–17) and malignant (18, 19) adrenocortical tumors and pheochromocytomas (13, 20, 21). The cellular adaptions at the metabolic level that occur during tumorigenesis and, in case of malignant disease, tumor progression and metastasis are elusive.

The ability of mass spectrometry imaging (MSI) to localize biomolecules in tissues without prior knowledge of their presence in various types of specimens has led to a rapid and substantial effect in clinical and pharmacological research by uncovering molecular changes associated with disease. A broad spectrum of analytes ranging from proteins, protein modifications, peptides, drugs and their related metabolites, endogenous cell metabolites, lipids, contrast agents, and other molecules have been made accessible by this *in situ* technique (22–24). By retaining information on the spatial localization of analytes beyond the mass spectrometry experiment, MSI permits the correlation of molecular information with the spatial information conveyed by conventional histology. Previous MSI studies using animal adrenal gland as model system focused only on specific molecular classes (*i.e.,* lipids, fatty acids, steroid hormones, catecholamines, cholesterol, or ascorbic acid) (25–31). Several mass spectrometry–based studies applied derivatization to enhance the signal intensity of endogenous steroid hormones (29, 32–34).

Here, we report a comprehensive MSI study of the human adrenal gland that encompasses a broad array of biomolecules, including catecholamines, sterol and steroid metabolites, energy-related nucleotides, metabolites of central energy pathways, lipids, and fatty acids by high-resolution matrix-assisted laser desorption/ionization–Fourier transform–ion cyclotron resonance (MALDI-FT-ICR) MSI. Six normal adrenal glands that include five fresh-frozen and one formalin-fixed paraffin-embedded (FFPE) tissues were integrated in this study. Molecules in common allowed reproducible clustering of molecular zones from different adrenal glands. Nevertheless, inter- and intrametabolic heterogeneity could also be observed at the level of pathway analyses between individuals. Pathway analyses of the different molecular zones defined by unsupervised clustering revealed predilection of different metabolic pathways for discrete substructures of the adrenal gland. Overall, *in situ* metabolite profiling resulted in a more detailed view of adrenal cortical zonation in comparison with classical histologic definitions. This molecular view of the normal adrenal gland may serve as a reference for understanding metabolic changes associated with disease and, in particular, metabolic adaptions during adrenal tumor development and progression.

Materials and Methods

Preparation of tissue samples

Five fresh-frozen normal adrenal glands were included in this study. The kidney transplantation donor adrenal (DAN) samples included DAN180 (male, age 23), DAN167 (male, age 20), DAN77 (female, age 26), DAN97 (male, age 2), and a renal cancer surgical adrenal sample (male, Wuerzburg, age 59). Donors or their families provided informed consent and the use of adrenal gland samples was approved by the institutional review boards of the University of Michigan. This study was performed as part of the European Network for the Study of Adrenal Tumors Registry and biorepository and approved by the ethics committee of the University of Würzburg (approval number 88/11). For the male sample (Wuerzburg, age 59), written informed consent was obtained from the patient. Tissue samples were immediately dissected, fresh-frozen in liquid nitrogen, and stored at −80°C until further processing.

One normal FFPE adrenal gland (male, age 49) from tumor nephrectomy was obtained from the Institute of Pathology, University Bern, Switzerland. FFPE samples were fixed for 12 hours in 10% neutral buffered formalin and then embedded in paraffin using standardized and automated procedures.

Tissue sectioning and matrix application

Fresh-frozen samples were cut into 12-μm sections such that a maximum of anatomical features was preserved by

using a cryomicrotome at −20°C (Leica CM1950; Leica Microsystems, Wetzlar, Germany) and mounted onto precooled conductive indium-tin-oxide–coated MALDI target glass slides (Bruker Daltonics, Bremen, Germany). FFPE tissue samples were sectioned with a thickness of 4 μm and water-bath–mounted onto indium-tin-oxide–coated glass slides (Bruker Daltonics). FFPE sections were incubated for 1 hour at 70°C, deparaffinized in xylene (2 × 8 minutes), and air dried. For MALDI-MSI of endogenous metabolites, the matrix solution was 10 mg/mL 9-aminoacridine hydrochloride monohydrate matrix (Sigma-Aldrich, Taufkirchen, Germany) in water/methanol 30:70 (v/v). The 9-aminoacridine hydrochloride monohydrate matrix was chosen as a matrix because it is known to exhibit very few matrix-derived interferences in the low-mass range and achieve high sensitivity and high linearity in negative ion mode for a wide range of low-molecular-weight metabolites (35–39). The matrix solution was sprayed on the tissue sections using a SunCollect automatic sprayer (Sunchrom; Friedrichsdorf, Germany) at room temperature. The matrix application was performed at flow rates of 10, 20, 30, and 40 μL/min, respectively, for the first four layers. The other four layers were performed at 40 μL/min.

MALDI-MSI experiment

Following tissue sample preparation, the MALDI-MSI measurement was performed on a Bruker Solarix 7T FT-ICR-MS (Bruker Daltonics). The MALDI-MSI data were acquired over a mass range of m/z 50 to 1000. Mass imaging data were acquired in negative ionization mode with 70-μm spatial resolution using 50 laser shots at a frequency of 500 Hz. After the MALDI-MSI measurement, the acquired data from the tissue samples underwent spectra processing in FlexImaging v. 4.2 (Bruker Daltonics).

Hematoxylin and eosin staining and histology

Following the MALDI imaging experiments, the matrix was removed with 70% ethanol. The tissue sections were stained with hematoxylin and eosin (H&E). Slides were scanned with a MIRAX DESK digital slide-scanning system (Carl Zeiss MicroImaging, Göttingen, Germany).

Immunohistochemistry

Frozen sections of human adrenal glands were cut at a thickness of 12 μm. Sections were fixed with cold acetone. After peroxidase blocking, primary antibody was applied to each section and slides were incubated at room temperature for 1 hour. The following primary antibodies and dilutions were used: aldosterone synthase [CYP11B2; mouse monoclonal, 1:100, Research Resource Identifier (RRID): AB_2650562] (40) and 11β-hydroxylase (CYP11B1; rat monoclonal, 1:50, RRID: AB_2650563) (40), both of which were provided by Dr. Celso E. Gomez-Sanchez, University of Mississippi Medical Center, and cytochrome b5 type A (CYB5A; Acris, Rockville, MD; catalog no. AM31963PU-N; mouse monoclonal, 1:5000, RRID: AB_11148731). The Envision plus system (Dako, Carpinteria, CA; catalog no. K4006) or Polink-2 plus detection kit (GBI Laboratories, Bothell, WA; catalog no. D46-18) was used for detection. Slides were counterstained with hematoxylin.

Bioinformatics and statistical analysis

MATLAB R2014b (v.7.10.0; Mathworks, Inc., Natick, MA) was used as a MALDI spectral preprocessing tool for the subsequent data bioinformatics analysis. Peak picking was performed as described in detail previously (41). Briefly, the parameters of peak picking included m/z 0.0005 minimal peak width, signal to noise threshold of 2 and intensity threshold of 0.01%. Isotopes were automatically identified and excluded. Statistical comparisons were performed with Student *t* test (two-tailed). $P \leq 0.05$ was considered statistically significant. Metabolites were considered to be significant if they had an intensity fold change ≥2 and $P \leq 0.05$. Heatmap-based clustering was created with MetaboAnalyst 3.0 (http://www.metaboanalyst.ca) (42). List of m/z species with respective intensities for regions of interest were uploaded to MetaboAnalyst and processed with a mass tolerance of m/z 0.0001 and no data filtering. The resulting heatmaps of metabolite data were exported as figures.

Unsupervised hierarchical clustering

Hierarchical clustering was performed using the built-in FlexImaging v. 4.2 (Bruker Daltonics) functionality, in which similar spectra are grouped using multivariate statistical analysis (43, 44). The created segmentation maps were then used to identify areas in which similar spectra occur across the tissue sample.

Metabolite annotation and pathway analysis

Metabolite annotation was performed by matching accurate mass with databases as previously described (39, 41, 45) [mass accuracy ≤4 ppm; METLIN, http://metlin.scripps.edu/; Human Metabolome Database, http://www.hmdb.ca/ (46); MassTRIX, http://masstrix3.helmholtz-muenchen.de/masstrix3/; METASPACE, http://annotate.metaspace2020.eu/ (47)].

Pathway analysis was applied to identify discriminative features of these histological zones of adrenal gland. The Kyoto Encyclopedia of Genes and Genomes (KEGG) database (http://www.genome.jp/kegg/) and MetaboAnalyst 3.0 (http://www.metaboanalyst.ca) were used. To do so, the average spectrum of each zone was compared with the average spectrum of cortex and medulla, respectively (*i.e.*, the average spectra of clusters 1 through 6 were compared with the average spectrum of the whole cortex; the average spectra of clusters 7 through 10 were compared with the average spectrum of the entire medulla). Masses with peak intensity fold change ≥2 were defined as discriminative masses of the corresponding cluster. The distinctively associated masses of each cluster were then annotated in metabolite databases, mapped into the KEGG pathways, and categorized into main metabolite classes.

On tissue MALDI–tandem mass spectrometry for the identification of metabolites

For identification of metabolites in adrenal gland tissue samples, on-tissue tandem mass spectometry (MS/MS) analysis was conducted using continuous accumulation of selected ions mode and collision-induced dissociation in the collision cell by MALDI-FT-ICR MS. Metabolites were identified by comparing the observed MS/MS spectra with standard compounds as previously described (39).

Results

Sample description and data acquired

Figure 1 summarizes five normal human adrenal glands used in this study. To assess functional adrenal

zonation, expression of zone-specific markers was examined using immunohistochemistry (IHC). The enzyme CYP11B2, which is required for aldosterone biosynthesis, was specifically expressed in the ZG, whereas the enzyme CYP11B1, which is needed for cortisol synthesis, was observed both in the ZF and ZR (40). CYB5A is a cofactor protein that enhances the 17, 20-lyase activity of 17α-hydroxylase and is required for dehydroepiandrosterone synthesis in the ZR (48). In IHC, CYB5A expression was localized to the ZR in adult adrenals. A clear morphological separation of cortex and medulla could be achieved through H&E and IHC staining. Because of the technical difficulty of obtaining complete anatomical features of adrenal gland, the section area of medulla varied between samples (*i.e.,* in DAN180, DAN97, and the Wuerzburg adrenal, a clear presence of medulla could be observed). In sample DAN167, only a small amount of medulla could be detected in the middle of the tissue section. In sample DAN77, no medulla was present. Therefore, selected samples were included in the heatmap-based cluster analyses and spatial segmentation mapping. Because the ZR is not fully developed in infant adrenals (48), limited CYB5A-expressing cells were observed in the 2-year-old's adrenal.

Overall, approximately 2000 individual MS peaks per pixel within the mass range of m/z 50 to 1000 could be resolved within the tissue examined. In total, 898 metabolites were annotated through Metaspace database (http://annotate.metaspace2020.eu/) (47), which covered 97 KEGG metabolic pathways (http://www.genome.jp/kegg/).

Targeted analysis of endogenous compounds within the human adrenal gland

To further investigate the metabolites represented in distinct histological zones of the adrenal gland, a comprehensive *in situ* distribution analysis of endogenous metabolites including catecholamines, sterol and steroid metabolites, nucleotide derivatives, intermediates of glycolysis and tricarboxylic acid (TCA) cycle, lipids and fatty acids was performed. All metabolites mentioned here were identified with on-tissue MS/MS analysis by comparing the observed MS/MS spectra with standard compounds or by matching accurate mass with databases as previously described (39, 41, 45) (Supplemental Data 1).

As demonstrated in Fig. 2, both epinephrine (m/z 182.0825) and norepinephrine (m/z 168.0667) were observed in the same overlapping areas of the adrenal medulla. Assuming a similar ionization, desorption and detection of epinephrine and norepinephrine observed intensities suggest an approximately three times lesser abundance of norepinephrine compared with epinephrine, which is very close to norepinephrine/epinephrine ratios reported previously from adrenal venous sampling (49).

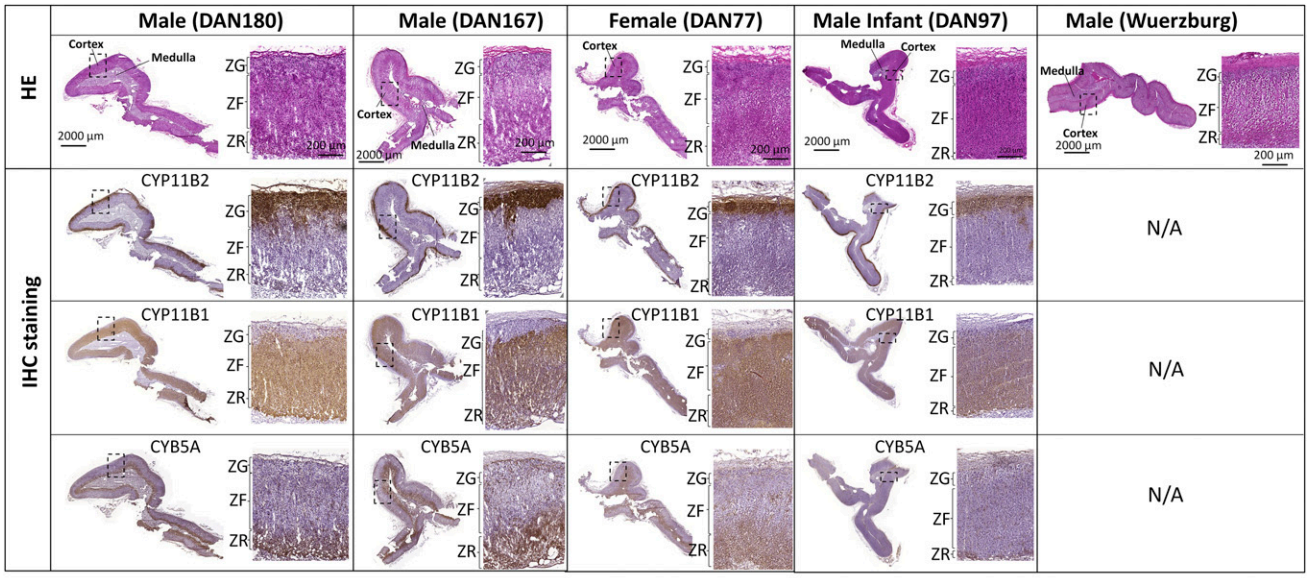

Figure 1. H&E and IHC staining of five human adrenal glands used in this study. A clearly immunophenotypic pattern of cortex and medulla could be achieved through H&E and IHC staining. Because of the technical difficulties of obtaining complete anatomical features of adrenal gland, the section of medulla varied between samples [*i.e.,* in DAN180 (male) DAN97 (male infant) and the Wuerzburg sample (male), an obvious presence of medulla could be observed]. In sample DAN167, a small amount of medulla could be detected in the middle of the tissue section. In sample DAN77 (female), no medulla was present. In IHC, the enzyme CYP11B2 was specifically expressed in the zona glomerulosa. The enzyme CYP11B1 was observed both in the ZF and ZR. CYB5A expression was observed in adult adrenal ZR. Because the ZR is less developed in infant adrenals, limited CYB5A-expressing cells were seen in the infant adrenal gland (DAN97). Note: The IHC of the Wuerzburg sample was not available.

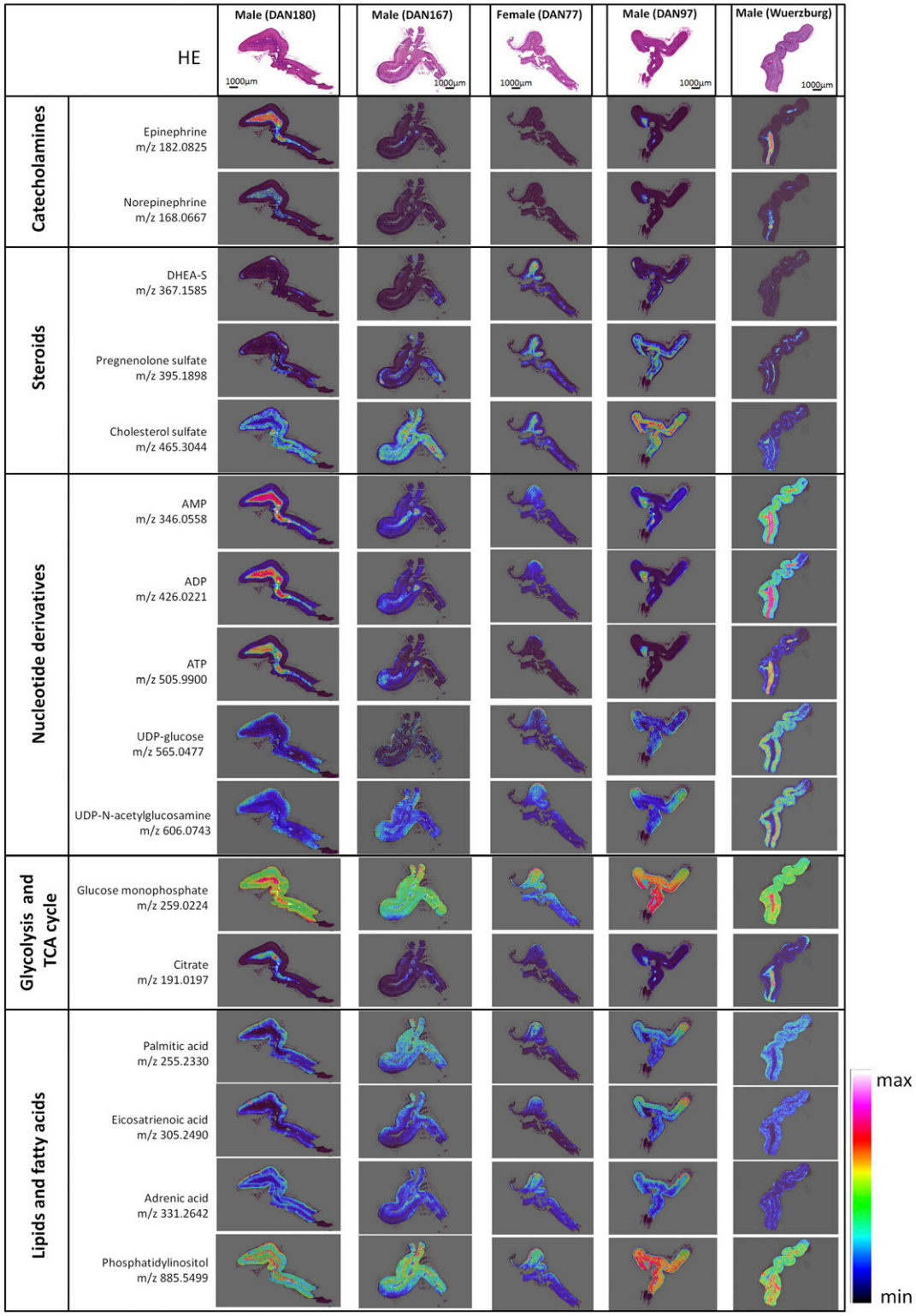

Figure 2. Examples of MSI scans of catecholamines, steroids, nucleotides, glycolysis, TCA cycle, lipids, and fatty acids. Epinephrine and norepinephrine are highly abundant in medulla, as expected, whereas steroid and sterol metabolites DHEA-S, pregnenolone sulfate, and cholesterol sulfate were detectable in cortex only. Nucleotides AMP, ADP, and ATP; glucose monophosphate; and citrate as representatives of glycolysis. TCA cycle showed high intensity in medulla. Of note, UDP-glucose and UDP-galactose were highly abundant in cortex. Palmitic acid and icosatrienoic acid were highly abundant in ZG and ZF. Adrenic acid was specifically localized in ZG and ZR. Phosphatidylinositol showed high intensity at the interface between cortex and medulla. ADP, adenosine 5′-diphosphate; AMP, adenosine 5′-monophosphate; ATP, adenosine triphosphate; DHEA-S, dehydroepiandrosterone sulfate; UDP, uridine diphosphate.

Whereas the catecholamines were strongly expressed in medulla, the sulfated steroids [*i.e.*, dehydroepiandrosterone sulfate (DHEA-S), pregnenolone sulfate, and cholesterol sulfate identified in this study] were expressed only in the cortex and showed different distributions between male and female adrenals. A detailed comparison (Fig. 3) shows that, in the female adrenal gland, DHEA-S was highly abundant in the ZR and colocalized with CYB5A, as expected. In contrast, DHEA-S had very low expression levels in male samples and was localized mainly in the ZF. A similar spatial distribution could be observed for pregnenolone sulfate, which was highly expressed in the ZR of the female adrenal gland and had low expression in male adrenal gland with a specific location in ZF and ZR. Cholesterol sulfate was highly abundant in both male and female adrenal glands, with heterogeneous distributions (*i.e.*, highly abundant in ZF and ZR in males; present in ZR solely in female). Next, we focused on nucleoside phosphates, highly representative endogenous metabolites in MALDI MSI experiments (Fig. 2). Mono, di-, and triphosphorylated nucleosides closely mirror the energetic state of a given cell and hence might provide an opportunity to study their role in the functionally distinct adrenal compartments. We found a discrete pattern of nucleotide distribution between the adrenal cortex and the medulla. Adenosine triphosphate (ATP), adenosine 5′-diphosphate (ADP), and adenosine 5′-monophosphate showed high intensity in the medulla, which is consistent with a highly active oxidative phosphorylation in the medulla (20). At variance, uridine diphosphate (UDP)-glucose and UDP-*N*-acetylglucosamine were located mainly in the outer adrenal cortex.

We next focused on the distribution of intermediates of glycolysis and the TCA cycle. In Fig. 2, we present the distribution profiles of glucose monophosphate (m/z 259.0224) and citrate (m/z 191.0197). Glucose monophosphate was found in both inner medulla and outer cortex, with heterogeneous intensities. Citrate was almost completely localized to the adrenal medulla.

Several lipids and fatty acids represented specific localization in different zones of adrenal gland (*e.g.*, palmitic acid and icosatrienoic acid were highly abundant in the ZG and ZF). Adrenic acid was specifically localized in the ZG and ZR. Phosphatidylinositol showed high intensity at the interface between cortex and medulla.

The heterogeneous distributions of these endogenous metabolites indicate a distinct molecular variance and suggest a series of molecular zones of adrenal gland that served as basis for further histopathological stratification.

Pathway and clustering analysis of the adrenal cortex and medulla

We next performed metabolic comparison of cortex and medulla. In this analysis, four adrenal glands (male DAN180, male DAN167, male infant DAN97, and male Wuerzburg) were included because no medulla was present in the fifth adrenal gland section (female DAN77). In total, 339 molecules were found to be significantly different between cortex and medulla (two-tailed Student *t* test $P \leq 0.05$, fold change ≥ 2). As an example, MSI images of six representative metabolites, which indicated distinct metabolic patterns between cortex and medulla, are shown in Fig. 4 (three enriched in cortex: palmitic acid, arachidonic acid,

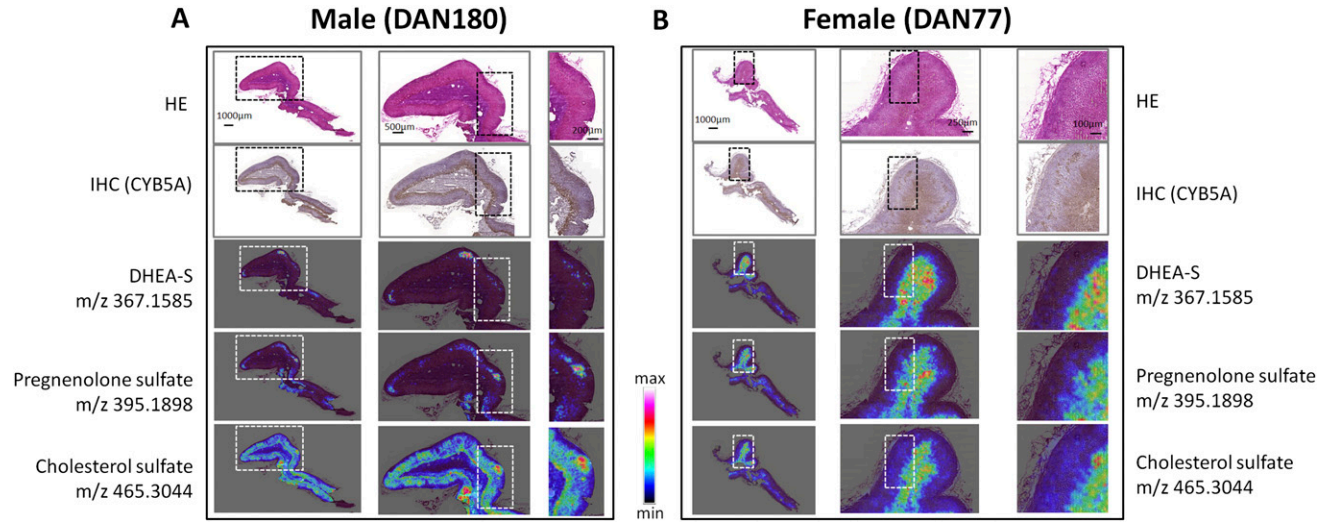

Figure 3. Comparison of sulfated steroids (DHEA-S, pregnenolone sulfate, and cholesterol sulfate) between male and female adrenal glands. MSI and IHC (CYB5A) images of three sulfated steroids (DHEA-S, pregnenolone sulfate, and cholesterol sulfate) are shown. In the female adrenal gland, DHEA-S was highly abundant in ZR and colocalized with CYB5A, whereas DHEA-S had a very low expression level in the male sample localized mainly in the ZF. Pregnenolone sulfate was highly expressed in the ZR in female adrenal gland and less expressed in the male adrenal gland, with a specific localization in ZF and ZR. Cholesterol sulfate was highly present in both male and female adrenal glands, with heterogeneous distributions (*i.e.*, highly abundant in ZF and ZR in the male samples, and solely present in the ZF in the female sample).

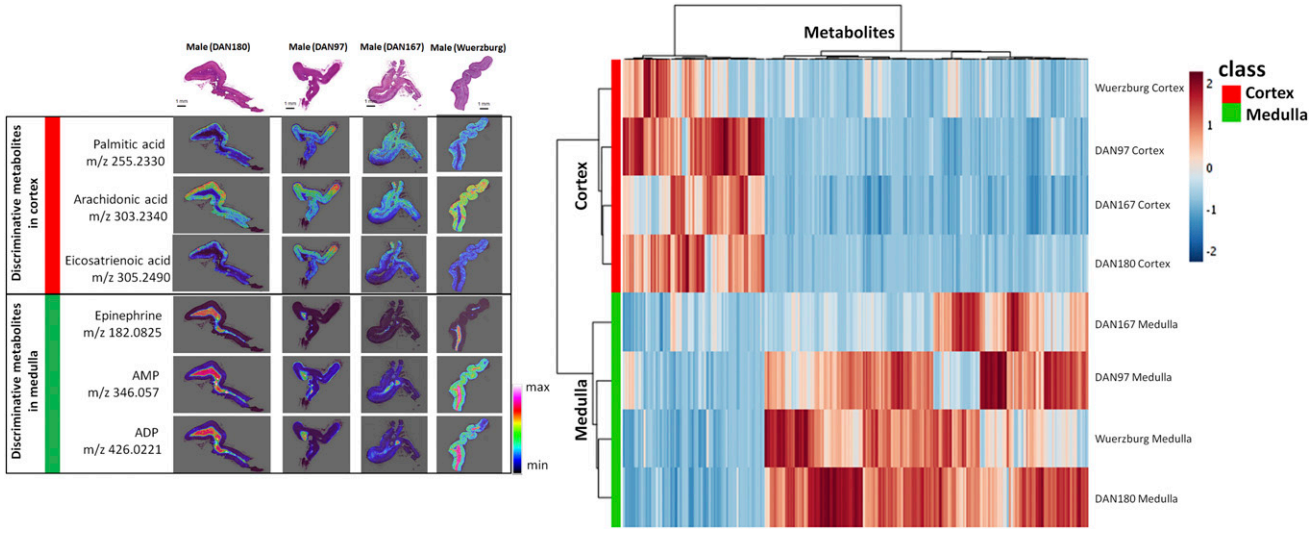

Figure 4. Discriminative metabolites and heatmap-based clustering analysis of the adrenal cortex and medulla. In this analysis, four adrenal glands (DAN180, DAN167, DAN97, and the Wuerzburg adrenal) were included, because no medulla was present in the fifth adrenal gland section (DAN77). (Left) From top to bottom: six metabolites discriminative in cortex (palmitic acid, arachidonic acid, and icosatrienoic acid) and medulla (epinephrine, AMP, and ADP) were represented as shown. (Right) Heatmap-based clustering analysis based on the discriminative metabolites (n = 339) represents a clear separation of cortex and medulla. AMP, adenosine 5′-monophosphate.

icosatrienoic acid; and three enriched in medulla: adrenalin, adenosine 5′-monophosphate, and ADP). Further heatmap-based clustering analysis based on the global metabolic profiles revealed a clear separation of cortex and medulla and good reproducibility between samples (Fig. 4). The metabolites responsible for the metabolic differentiation were then subjected to pathway enrichment analysis. Modulated pathways in cortex and medulla are listed in Table 1. As a result, we found lipid metabolism, including biosynthesis of unsaturated fatty acids, fatty acid biosynthesis, linoleic acid metabolism, glycerophospholipid metabolism, and steroid hormone biosynthesis, to be highly enriched in cortex. The aldosterone synthesis and secretion pathway were also increased in the cortex. At variance, the carbohydrate metabolism (including pentose phosphate pathway, pentose and glucuronate interconversions, glycolysis/gluconeogenesis, and glucose and mannose metabolism), glucagon signaling pathway, amino acid metabolism, and nucleotide metabolism were significantly increased in medulla.

Spatial segmentation of histological components through unsupervised hierarchical clustering

Hierarchical clustering is a commonly used computational data-mining method for MALDI imaging data

Table 1. Modulated Metabolic Pathways in the Adrenal Cortex and Medulla

	Pathways	Cortex	Medulla
Lipid metabolism	Biosynthesis of unsaturated fatty acids	+	−
	Linoleic acid metabolism	+	−
	Fatty acid biosynthesis	+	−
	Glycerophospholipid metabolism	+	−
	Steroid hormone biosynthesis	+	−
	Inositol phosphate metabolism	−	+
Carbohydrate metabolism	Pentose phosphate pathway	−	+
	Pentose and glucuronate interconversions	−	+
	Glycolysis/gluconeogenesis	−	+
	Fructose and mannose metabolism	−	+
Endocrine system	Aldosterone synthesis and secretion	+	
	Glucagon signaling pathway	−	+
Amino acid metabolism	Tyrosine metabolism	−	+
	Phenylalanine, tyrosine, and tryptophan biosynthesis	−	+
Nucleotide metabolism	Purine metabolism	−	+

The metabolites responsible for the metabolic differentiation between cortex and medulla were subjected to pathway analysis. A list of discriminative pathways is shown.

Abbreviations: +, upregulated pathways; −, downregulated pathways.

analysis (24, 43, 44, 50–52) that has proven its potential in histological analysis of cancer tissues (24, 50, 53, 54). To decipher anatomical structures of the adrenal gland in more detail, the MSI data were subjected to a *de novo* discovery approach using unsupervised hierarchical clustering analysis, in which the individual spectra of each data set were grouped according to their spectral similarity (43, 44). Figure 5 represents a spatial segmentation map based on unsupervised hierarchical clustering of three adrenal glands (male DAN180, male infant DAN97, and male Wuerzburg).

As a result, a graphical representation of anatomical structures defined by molecular patterns was obtained (Fig. 5). Clearcut separation between the adrenal medulla and cortex was reached (Fig. 5, cluster level 1). A virtually perfect match of this molecular based map with established histological morphological features of the adrenal gland composed of ZG, ZF, ZR and medulla was observed (Fig. 5, cluster level 2). This led us to conclude that the number and the physicochemical properties of the analytes retrieved by MALDI-MSI were sufficient to reproduce previously known structures.

By exploiting the wealth of molecular data generated by MALDI-MSI, we next aimed to provide a more detailed characterization of the adrenal gland by describing domains defined at the molecular level. Further improved spatial segmentation map through unsupervised hierarchical clustering of human adrenal gland created molecular zones that opened aspects that are not completely reflected by the classic histological layers of the adrenal gland (Fig. 5, cluster level 3). The clustering result represents 10 individual molecular zones of the adrenal gland, in which molecular zones 1 through 6 represent cortex substructures and molecular zones 7 through 10 compartments of the medulla (Fig. 5, cluster level 3). A good reproducibility of the classification of molecular subzones could be achieved between individuals. It should be noted that the ZR was less developed in infant adrenal, resulting in a limited ZR for metabolic profiling. Therefore, further clustering of ZR in infant adrenal gland (male infant DAN97) was unfeasible.

Bioinformatics pathway analysis of functional molecular zones of adrenal gland

Pathways enriched in the adrenal capsule include "biosynthesis of unsaturated fatty acids," "glycerophospholipid

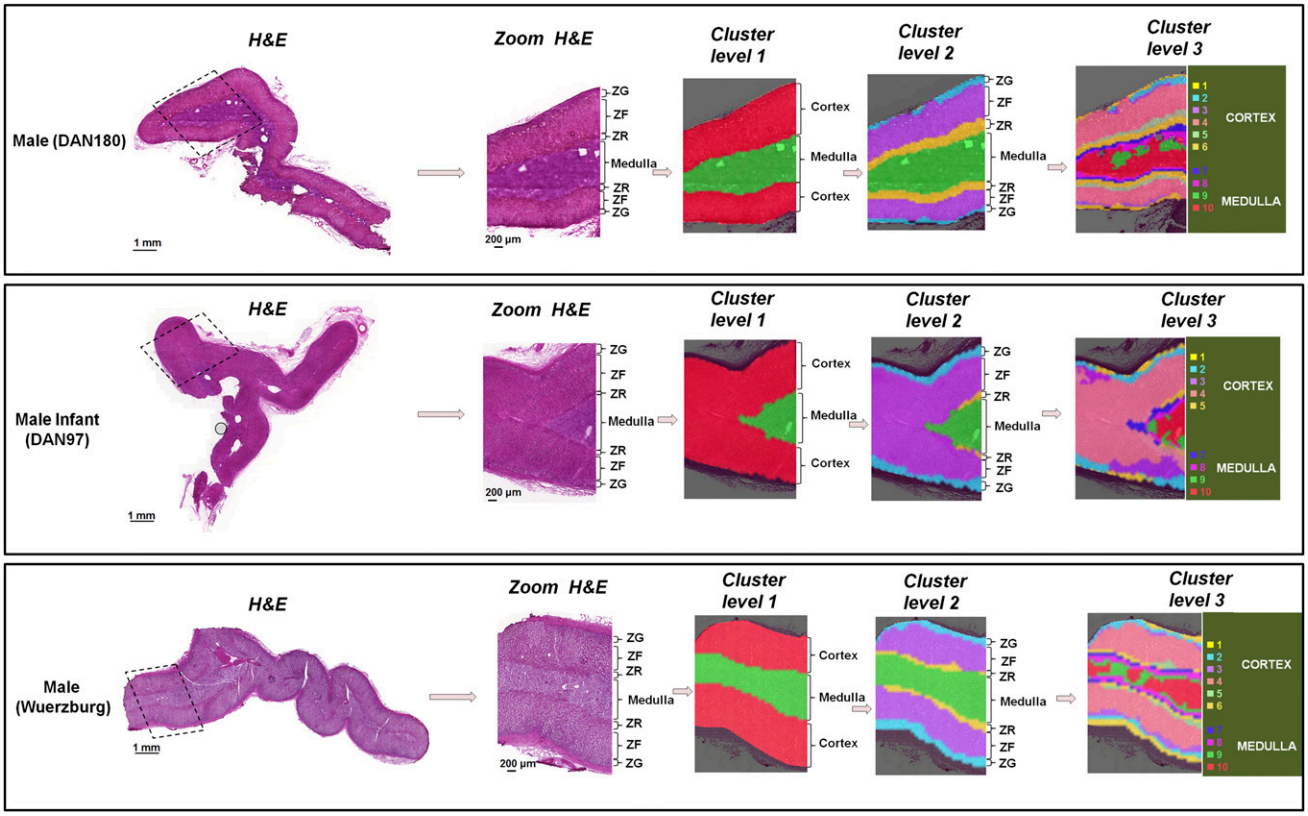

Figure 5. Spatial segmentation map based on unsupervised hierarchical clustering of three adrenal glands (DAN180, DAN97, and the Wuezburg sample). H&E images with zoomed regions of cortex and medulla are shown. The spatial segmentation map based on unsupervised hierarchical clustering aligned well with the morphological features of adrenal gland, including ZG, ZF, ZR, and medulla. An improved spatial segmentation map through unsupervised hierarchical clustering of human adrenal gland created molecular zones, which suggest intracortical regions with distinct metabolic profiles. Molecular zones 1 through 6 represented the cortex area; molecular zones 7 through 10 corresponded to the medulla area. A good reproducibility of the classification of molecular subzones was achieved between individuals. Note the limited ZR in the infant adrenal gland sample, precluding subclustering of ZR in this specimen.

metabolism," "phosphatidylinositol signaling system," and "amino sugar and nucleotide sugar metabolism." Discriminative changes of metabolism could be observed in the distinct molecular zones defined in Fig. 5 (zones 1 through 6 of the cortex area; zones 7 through 10 of the medulla area). The metabolites responsible for these distinct molecular zones were subjected to bioinformatics pathway analysis. Figures 6 and 7 summarize discriminative pathways of corresponding molecular zones in cortex and medulla, respectively. Classes of metabolites with a high number of variations are carbohydrate metabolism, lipid metabolism, amino acid metabolism, and endocrine system (Figs. 6 and 7). Both intra- and interheterogeneity between distinct molecular zones and individuals could be observed at the level of pathway analyses. It is noteworthy that the interface zones between the cortex and the medulla (zones 6 and 7) exhibits profound changes of discriminative pathways (Figs. 6 and 7).

Stratification of FFPE adrenal glands

In clinical routine diagnostics, FFPE tissue specimens are widely available, whereas analysis of fresh-frozen tumor samples requires additional diagnostic workflows. Previous publications have demonstrated the ability to measure metabolites in FFPE tissues using MALDI-FT-ICR MSI, which can then be assigned to histology and clinical parameters (41, 55). Here we performed proof-of-principle clustering analysis using FFPE human adrenal glands to explore the feasibility of the stratification approach on FFPE tissue and obtain insight about similarities and differences in metabolites detected. Overall, ~2000 individual MS peaks per pixel within the mass range of m/z 50 to 1000 were recorded, of which 279 metabolites were annotated through the Metaspace database (47). These covered 46 KEGG metabolic pathways. Despite the lower analyte coverage of FFPE tissue, we were able to perform the stratification approach on FFPE adrenal glands and found six molecular-defined regions representative of ZG, ZF, and ZR, respectively. Taken together, our results indicate the potential to transfer statistical clustering analyses also to FFPE tissue and infer histological zones statistically without knowledge of their morphologic correlate (Supplemental Data 2).

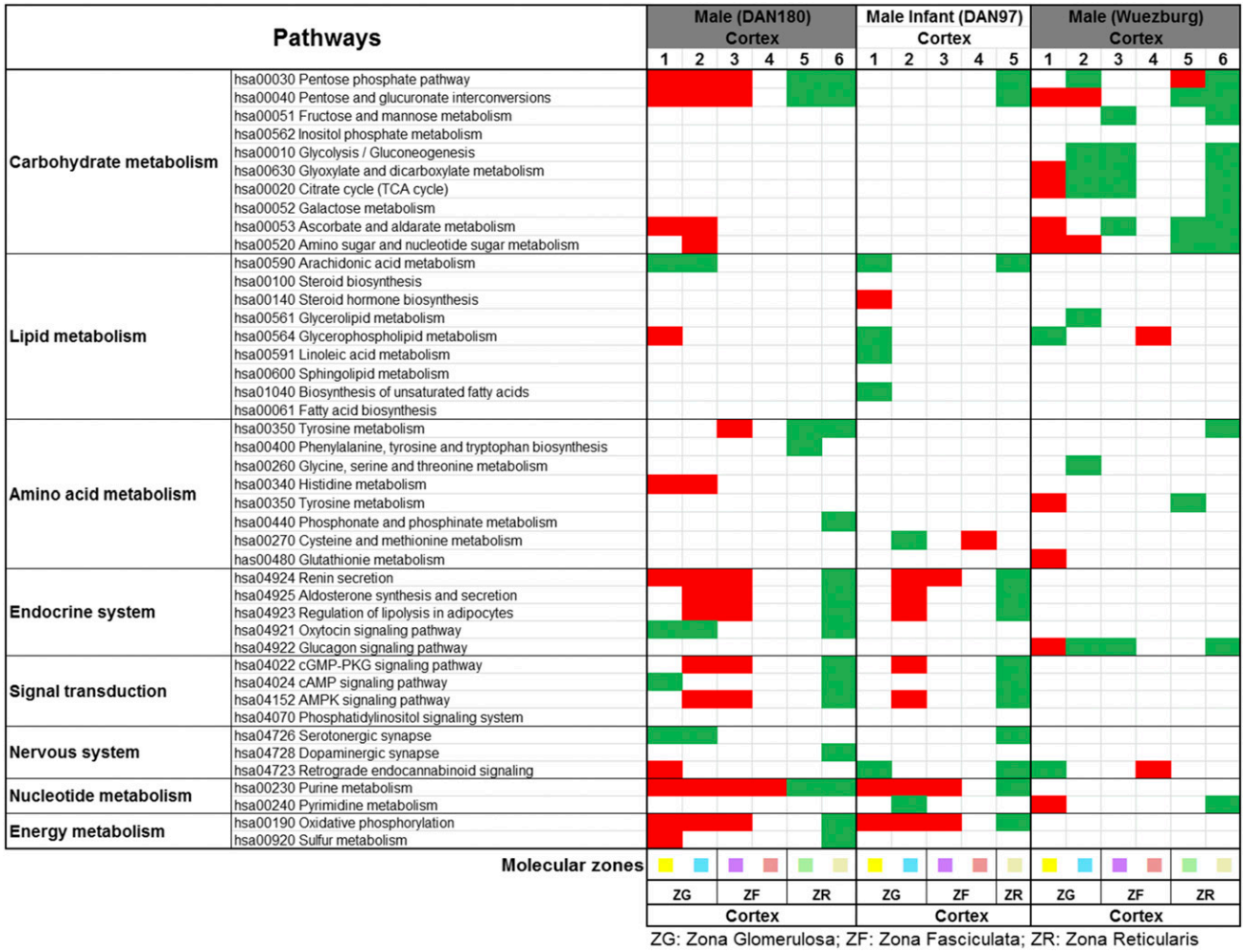

Figure 6. Discriminative pathways of corresponding molecular zones in the adrenal cortex. Red indicates downregulated pathways; green indicates upregulated pathways.

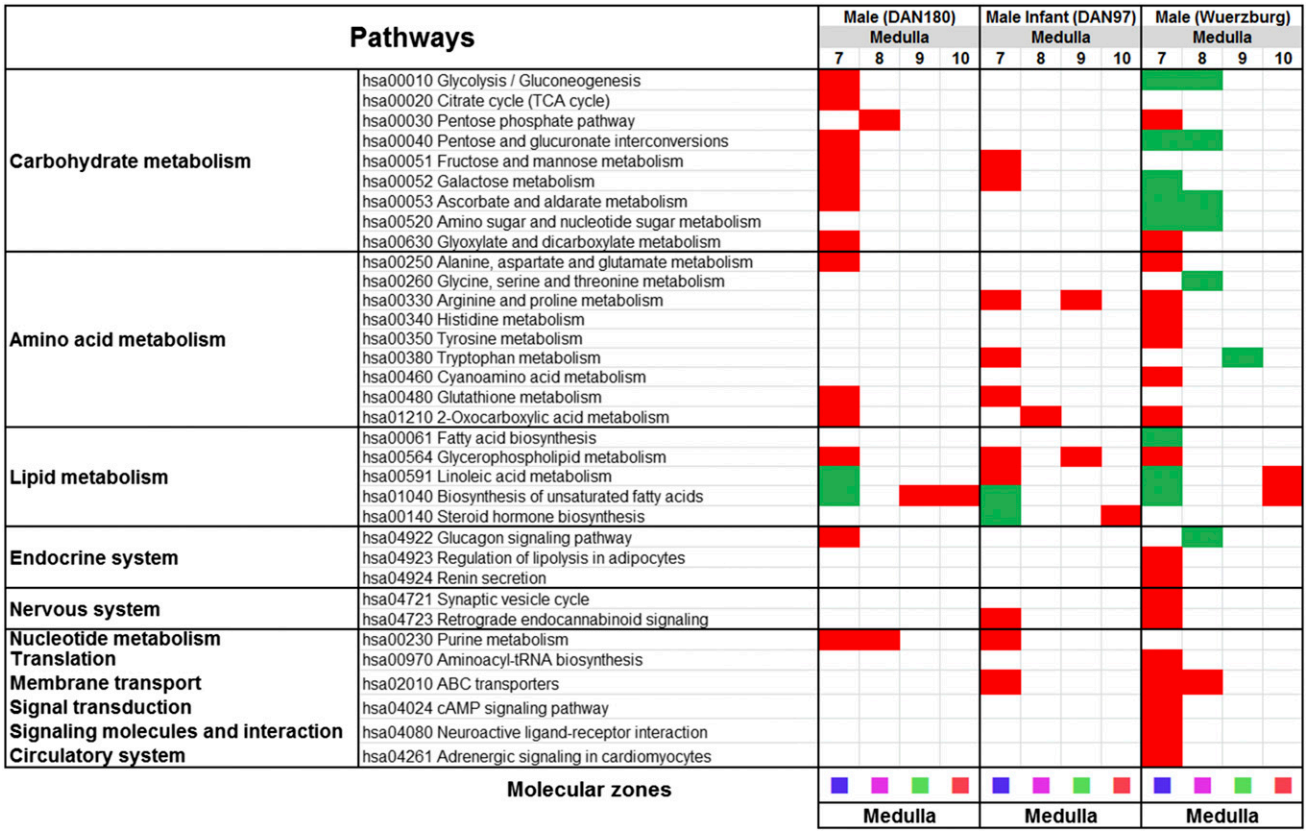

Figure 7. Discriminative pathways of corresponding molecular zones in the adrenal medulla. Red indicates downregulated pathways; green indicates upregulated pathways.

Discussion

A combined approach of MALDI metabolite imaging and immunohistochemical staining of functional adrenal zonation in human was applied to correlate histological features and molecular properties at microscopic level. The high-resolution MALDI-MSI allows a visual analysis of spatial information from a broad range of metabolites in the human adrenal gland. To assess functional adrenal zonation, expression of zone-specific markers was examined using IHC. The results provide findings that indicate varying metabolic activities with respect to the histological structures of adrenal gland. Combination of both molecular informed and histologic approaches revealed the exact colocalization of sulfated sterol steroid hormone with an IHC marker specific for adrenal gland zones. Thus, DHEA-S was visualized in complete accordance with the expression of the ZR-specific CYB5A protein (Fig. 3). Further, we were able to characterize a molecular adrenal anatomy based on both the level of individual analytes as well as alterations in comprehensive metabolic pathways. Finally, we could define functional molecular zones of human adult adrenal gland structure beyond classical histological anatomy.

In previous studies, Wu *et al.* and Wang *et al.* reported molecule imaging of porcine adrenal glands including lipids, fatty acids, epinephrine, norepinephrine, and cholesterol as examples (25, 26). Here, we present a comprehensive metabolic imaging study of human adrenal glands that covers global metabolic pathways, including carbohydrate metabolism, energy metabolism, lipid metabolism, amino acid metabolism, endocrine system, nucleotide metabolism, and signal transduction. The heterogeneous localization patterns of the key metabolites including catecholamines, sterol and steroid metabolites, nucleotides, central metabolism pathway intermediates, lipids, and fatty acids could be observed. Compared with previous findings in porcine adrenal glands (25), similar distributions of catecholamines could be observed, with main localizations in medulla. In our approach to differentiate male and female samples, we observed distinct distribution patterns of DHEA-S in male and female adrenal glands. In the female, DHEA-S was highly abundant in ZR; however, in the males, DHEA-S presented with very low intensity and localized mainly in the ZF. DHEA-S is a testosterone precursor produced in greatest quantities by the adrenal cortex and counts among the weak androgens that are formed from puberty onward in humans. In males, the amount released from the adrenal glands and converted to testosterone is physiologically insignificant compared with the amount secreted by the testes but, in females, adrenal-derived

testosterone and testosterone precursors are important in maintaining normal pubic and axillary hair (56). Here we could identify significantly higher level of DHEA-S in adrenal glands in the female compared with the male samples, which was in the line with the physiological characteristics of males and females.

This study visualizes DHEA-S *in situ*, which showed excellent correlation with the corresponding enzymes. Hence MALDI-MSI can be expected to greatly contribute to an improved understanding of the physiology of androgen synthesis and metabolism throughout life from infants to adolescents to adult males and females, which is unprecedented in terms of spatial resolution. It is conceivable that MALDI-MSI will be useful to study androgen synthesis and related metabolic processes in animal models of adrenal steroidogenesis.

The high abundance of adrenic acid in the adrenal cortex is an unexpected finding of this study. Adrenic acid (docosatetraenoic acid) is identical to arachidonic acid except for two additional carbons on the carboxyl terminus. Adrenic acid is metabolized by cyclooxygenases, cytochrome P450s, and lipoxygenases. A previous study using bovine adrenals as a model system indicated that adrenic acid metabolites could function as ZG-derived hyperpolarizing factors in the adrenal cortex and contribute to the regulation of adrenal blood flow (57, 58). Little is known regarding the role of adrenic acid in the human adrenal gland. Our finding of high abundance both in the ZG and ZR by MALDI-MSI points to a broader role of adrenic acid in adrenal cortex physiology.

The high levels of both UDP-glucose and UDP-*N*-acetyl glucosamine in the cortex reflect high activity of glycogen synthesis and glycosylation. Glycogenolysis is known to be activated in response to ACTH stimulation of ZF and likely also angiotensin-II stimulation of ZG cells (59–64). However, the functional consequences and regulation of glycogen metabolism in adrenocortical cell function are poorly understood and have not attracted scientific attention in recent years. The specific role of glycosylation in the adrenal cortex and its potential interrelationship with energy status has not been described to our knowledge, but merits further investigation. Key metabolites of the TCA cycle are overrepresented in the medulla, reflecting active glycolysis required for oxidative phosphorylation. In distinct areas of the cortex that morphologically correspond to the ZG and part of the ZF, glucose monophosphate and fructose-1,6-bisphosphate are readily detectable, whereas TCA cycle intermediates are less prominently represented, which may point toward a less active TCA cycle and diversion of intermediates of glycolysis toward other cellular processes.

Molecular informed clustering tools demonstrate that the segmentation approach can be applied to evaluation of histological samples. A distinct separation of cortex and medulla could be observed both at the level of individual metabolite and comprehensive metabolic pathway levels. We observed elevated steroid hormone biosynthesis, aldosterone synthesis and secretion, and fatty acid biosynthesis in adrenal cortex. These results confirmed the biological function of adrenal cortex as a source of steroid hormones. In contrast, the medulla functions to produce a rapid response throughout the body in stress situations, in which highly active oxidative phosphorylation and energy consumption are demanded (20). Pathway enrichment analyses indicated enhanced activity of pentose phosphate pathway, glycolysis, and nucleotide metabolism (nucleoside triphosphates) in the medulla, likely reflecting the high energy consumption in medulla.

In comparison with the classical histoanatomic definition of human adrenal gland, molecular zones could be observed through clustering analysis, which permits unprecedented insight into differential activities of functional processes in the adrenal gland. There is clinical and molecular evidence supporting a functional role of the corticomedullary interaction in the adrenal gland during stress response (65, 66). Discriminative changes of metabolism can be observed in distinct molecular zones, most prominently in the corticomedullary interface zones (Fig. 4). Although the relevance of this molecular-based zonation remains to be elucidated, it is likely that it reflects functional adaptions possibly related to the known interplay between the adrenal medulla and cortex (65, 67). The anatomical underpinnings of this interaction are ill defined. Notably, both intra- and interindividual heterogeneity of molecular patterns was observed. This is already evident at the level of individual analytes and pathways. Although we cannot exclude that some of this heterogeneity is caused by sample processing and storage, we consider the majority of these changes to be related to functional adaption's role in the endocrine system as a response to internal physiology processes and environments that also may include direct effects of chemokines (68, 69) or Toll-like receptors, as during sepsis (70). The observation of intra-adrenal heterogeneity is a piece of evidence underscoring high molecular complexity within the currently classified histologic zones of the adrenal. The potential of the metabolically distinct zones to play important roles in adrenal steroid production as a response to physiology and environmental factors warrants further research.

MALDI-MSI provides unprecedented insight in the complex interplay of steroid- and catecholamine-producing adrenocortical tissue in the human adrenal gland and, in particular, molecular pathways that have not yet been related to adrenal gland function. An

Appendix. Antibody Table

Target	Antigen Sequence	Name of Antibody	Manufacturer, Catalog No., or Name of Individual Providing Antibody	Species Raised in; Monoclonal or Polyclonal	Dilution Used	RRID
CYP11B2	MPQHPGNRWLRL-C	AntihCYP11B2 antibody, clone 41-17B	Dr. C.E. Gomez-Sanchez (University of Mississippi Medical Center)	Mouse; monoclonal	1:100	AB_2650562
CYP11B1	YDLGGAGMVC	AntihCYP11B1 antibody, clone 80-2-2	Dr. C.E. Gomez-Sanchez (University of Mississippi Medical Center)	Rat; monoclonal	1:50	AB_2650563
CYB5A	AA 1-135	Anti-cytochrome b5 (1-135) antibody, clone 1A8	Acris, AM31963PU-N	Mouse; monoclonal	1:5000	AB_11148731

improved understanding of the relevance of metabolite profiles and physiological function may lead to improved understanding of disease mechanisms relevant to the human response to stress and will be particularly helpful as a reference to dissect metabolic pathways involved in the development of adrenal tumors, their growth, and progression.

Acknowledgments

The authors thank Claudia-Marieke Pflüger, Ulrike Buchholz, Gabriele Mettenleiter, and Andreas Voss from the Research Unit Analytical Pathology for providing technical assistance and Martina Zink from the University Hospital Würzburg for excellent management of the tissue bank. We are indebted to Felix Beuschlein and Martin Reincke, Munich, for valuable discussion.

Financial Support: A.W. was funded by the Ministry of Education and Research of the Federal Republic of Germany (Grants 01ZX1310B and 01KT16015) and the Deutsche Forschungsgemeinschaft (Grants SFB 824 TP Z02/C4 and CRC/TRR 205 S01). M.K. and M.F. were funded by the Deutsche Forschungsgemeinschaft (KR4371/1-1, FA 466/4-1, and CRC/TRR 2015 B16 and S02). M.K. was funded by a fellowship of the Comprehensive Cancer Center Mainfranken. A.W., M.K., and M.F. received funding from the Deutsche Krebshilfe (no. 70112617). K.N. was funded by a grant from the American Heart Association (17SDG33660447). W.E.R. was funded by a grant from the National Institute of Diabetes and Digestive and Kidney Diseases (DK106618).

Correspondence: Axel Walch, MD, Research Unit Analytical Pathology, Helmholtz Zentrum München, German Research Center for Environmental Health (GmbH), Ingolstädter Landstrasse 1, 85764 Neuherberg, Germany. E-mail: axel.walch@helmholtz-muenchen.de.

Disclosure Summary: The authors have nothing to disclose.

References

1. Ross MH, Pawlina W. *Histology: A Text and Atlas: With Correlated Cell and Molecular Biology*. 6th ed. Philadelphia: Wolters Kluwer/Lippincott Williams & Wilkins Health; 2011:974.
2. Melmed S, Polonsky KS, Larsen PR, Kronenberg H. *Williams Textbook of Endocrinology*. 13th ed. Philadelphia, PA: Elsevier; 2011:490–555.
3. Miller WL, Auchus RJ. The molecular biology, biochemistry, and physiology of human steroidogenesis and its disorders. *Endocr Rev*. 2011;**32**(1):81–151.
4. Jefferies WM. *Safe Uses of Cortisol*. 3rd ed. Springfield, IL.: Charles C Thomas; 2004:25–32.
5. Young B, O'Dowd G, Woodford P. *Wheater's Functional Histology: A Text and Colour Atlas*. 6th ed. Philadelphia, PA: Churchill Livingston/Elsevier; 2014:318–336.
6. Vinson GP, Whitehouse B, Hinson J. *The Adrenal Cortex*. *Prentice Hall Endocrinology Series*. Englewood Cliffs, NJ: Prentice Hall; 1992:1–316.
7. Porth C. *Pathophysiology: Concepts of Altered Health States*. 7th ed. Philadelphia: Lippincott Williams & Wilkins; 2005:1–1582.
8. Bornstein SR, Allolio B, Arlt W, Barthel A, Don-Wauchope A, Hammer GD, Husebye ES, Merke DP, Murad MH, Stratakis CA, Torpy DJ. Diagnosis and treatment of primary adrenal insufficiency: an Endocrine Society Clinical Practice Guideline. *J Clin Endocrinol Metab*. 2016;**101**(2):364–389.
9. Husebye ES, Allolio B, Arlt W, Badenhoop K, Bensing S, Betterle C, Falorni A, Gan EH, Hulting AL, Kasperlik-Zaluska A, Kämpe O, Løvås K, Meyer G, Pearce SH. Consensus statement on the diagnosis, treatment and follow-up of patients with primary adrenal insufficiency. *J Intern Med*. 2014;**275**(2):104–115.
10. Nieman LK. Cushing's syndrome: update on signs, symptoms and biochemical screening. *Eur J Endocrinol*. 2015;**173**(4):M33–M38.
11. Krone N, Dhir V, Ivison HE, Arlt W. Congenital adrenal hyperplasia and P450 oxidoreductase deficiency. *Clin Endocrinol (Oxf)*. 2007;**66**(2):162–172.
12. Fassnacht M, Kroiss M, Allolio B. Update in adrenocortical carcinoma. *J Clin Endocrinol Metab*. 2013;**98**(12):4551–4564.
13. Favier J, Amar L, Gimenez-Roqueplo AP. Paraganglioma and phaeochromocytoma: from genetics to personalized medicine. *Nat Rev Endocrinol*. 2015;**11**(2):101–111.
14. Choi M, Scholl UI, Yue P, Björklund P, Zhao B, Nelson-Williams C, Ji W, Cho Y, Patel A, Men CJ, Lolis E, Wisgerhof MV, Geller DS, Mane S, Hellman P, Westin G, Åkerström G, Wang W, Carling T, Lifton RPK. K+ channel mutations in adrenal aldosterone-producing adenomas and hereditary hypertension. *Science*. 2011; **331**(6018):768–772.
15. Beuschlein F, Boulkroun S, Osswald A, Wieland T, Nielsen HN, Lichtenauer UD, Penton D, Schack VR, Amar L, Fischer E, Walther A, Tauber P, Schwarzmayr T, Diener S, Graf E, Allolio B, Samson-Couterie B, Benecke A, Quinkler M, Fallo F, Plouin PF, Mantero F, Meitinger T, Mulatero P, Jeunemaitre X, Warth R, Vilsen B, Zennaro MC, Strom TM, Reincke M. Somatic mutations in ATP1A1 and ATP2B3 lead to aldosterone-producing adenomas and secondary hypertension. *Nat Genet*. 2013;**45**(4):440–444e2.

16. Beuschlein F, Fassnacht M, Assié G, Calebiro D, Stratakis CA, Osswald A, Ronchi CL, Wieland T, Sbiera S, Faucz FR, Schaak K, Schmittfull A, Schwarzmayr T, Barreau O, Vezzosi D, Rizk-Rabin M, Zabel U, Szarek E, Salpea P, Forlino A, Vetro A, Zuffardi O, Kisker C, Diener S, Meitinger T, Lohse MJ, Reincke M, Bertherat J, Strom TM, Allolio B. Constitutive activation of PKA catalytic subunit in adrenal Cushing's syndrome. *N Engl J Med*. 2014; **370**(11):1019–1028.
17. Assié G, Libé R, Espiard S, Rizk-Rabin M, Guimier A, Luscap W, Barreau O, Lefèvre L, Sibony M, Guignat L, Rodriguez S, Perlemoine K, René-Corail F, Letourneur F, Trabulsi B, Poussier A, Chabbert-Buffet N, Borson-Chazot F, Groussin L, Bertagna X, Stratakis CA, Ragazzon B, Bertherat J. ARMC5 mutations in macronodular adrenal hyperplasia with Cushing's syndrome. *N Engl J Med*. 2013; **369**(22):2105–2114.
18. Assié G, Letouzé E, Fassnacht M, Jouinot A, Luscap W, Barreau O, Omeiri H, Rodriguez S, Perlemoine K, René-Corail F, Elarouci N, Sbiera S, Kroiss M, Allolio B, Waldmann J, Quinkler M, Mannelli M, Mantero F, Papathomas T, De Krijger R, Tabarin A, Kerlan V, Baudin E, Tissier F, Dousset B, Groussin L, Amar L, Clauser E, Bertagna X, Ragazzon B, Beuschlein F, Libé R, de Reyniès A, Bertherat J. Integrated genomic characterization of adrenocortical carcinoma. *Nat Genet*. 2014;**46**(6):607–612.
19. Zheng S, Cherniack AD, Dewal N, Moffitt RA, Danilova L, Murray BA, Lerario AM, Else T, Knijnenburg TA, Ciriello G, Kim S, Assie G, Morozova O, Akbani R, Shih J, Hoadley KA, Choueiri TK, Waldmann J, Mete O, Robertson AG, Wu HT, Raphael BJ, Shao L, Meyerson M, Demeure MJ, Beuschlein F, Gill AJ, Sidhu SB, Almeida MQ, Fragoso MCBV, Cope LM, Kebebew E, Habra MA, Whitsett TG, Bussey KJ, Rainey WE, Asa SL, Bertherat J, Fassnacht M, Wheeler DA, Hammer GD, Giordano TJ, Verhaak RGW; Cancer Genome Atlas Research Network. Comprehensive pan-genomic characterization of adrenocortical carcinoma [published correction appears in *Cancer Cell*. 2016;30(2):363]. *Cancer Cell*. 2016;**29**(5):723–736.
20. Dahia PL. Pheochromocytoma and paraganglioma pathogenesis: learning from genetic heterogeneity. *Nat Rev Cancer*. 2014;**14**(2): 108–119.
21. Fishbein L, Leshchiner I, Walter V, Danilova L, Robertson AG, Johnson AR, Lichtenberg TM, Murray BA, Ghayee HK, Else T, Ling S, Jefferys SR, de Cubas AA, Wenz B, Korpershoek E, Amelio AL, Makowski L, Rathmell WK, Gimenez-Roqueplo AP, Giordano TJ, Asa SL, Tischler AS, Pacak K, Nathanson KL, Wilkerson MD; Cancer Genome Atlas Research Network. Comprehensive molecular characterization of pheochromocytoma and paraganglioma. *Cancer Cell*. 2017;**31**(2):181–193.
22. Balluff B, Schöne C, Höfler H, Walch A. MALDI imaging mass spectrometry for direct tissue analysis: technological advancements and recent applications. *Histochem Cell Biol*. 2011;**136**(3): 227–244.
23. Norris JL, Caprioli RM. Analysis of tissue specimens by matrix-assisted laser desorption/ionization imaging mass spectrometry in biological and clinical research. *Chem Rev*. 2013;**113**(4):2309–2342.
24. Walch A, Rauser S, Deininger SO, Höfler H. MALDI imaging mass spectrometry for direct tissue analysis: a new frontier for molecular histology. *Histochem Cell Biol*. 2008;**130**(3):421–434.
25. Wu C, Ifa DR, Manicke NE, Cooks RG. Molecular imaging of adrenal gland by desorption electrospray ionization mass spectrometry. *Analyst (Lond)*. 2010;**135**(1):28–32.
26. Wang X, Han J, Pan J, Borchers CH. Comprehensive imaging of porcine adrenal gland lipids by MALDI-FTMS using quercetin as a matrix. *Anal Chem*. 2014;**86**(1):638–646.
27. Vidová V, Novák P, Strohalm M, Pól J, Havlícek V, Volný M. Laser desorption-ionization of lipid transfers: tissue mass spectrometry imaging without MALDI matrix. *Anal Chem*. 2010;**82**(12): 4994–4997.
28. Malmberg P, Jennische E, Nilsson D, Nygren H. High-resolution, imaging TOF-SIMS: novel applications in medical research. *Anal Bioanal Chem*. 2011;**399**(8):2711–2718.
29. Cobice DF, Mackay CL, Goodwin RJ, McBride A, Langridge-Smith PR, Webster SP, Walker BR, Andrew R. Mass spectrometry imaging for dissecting steroid intracrinology within target tissues. *Anal Chem*. 2013;**85**(23):11576–11584.
30. Manier ML, Spraggins JM, Reyzer ML, Norris JL, Caprioli RM. A derivatization and validation strategy for determining the spatial localization of endogenous amine metabolites in tissues using MALDI imaging mass spectrometry. *J Mass Spectrom*. 2014;**49**(8): 665–673.
31. Wu C, Ifa DR, Manicke NE, Cooks RG. Rapid, direct analysis of cholesterol by charge labeling in reactive desorption electrospray ionization. *Anal Chem*. 2009;**81**(18):7618–7624.
32. Higashi T, Yamauchi A, Shimada K. 2-hydrazino-1-methylpyridine: a highly sensitive derivatization reagent for oxosteroids in liquid chromatography-electrospray ionization-mass spectrometry. *J Chromatogr B Analyt Technol Biomed Life Sci*. 2005;**825**(2): 214–222.
33. Wang Y, Hornshaw M, Alvelius G, Bodin K, Liu S, Sjövall J, Griffiths WJ. Matrix-assisted laser desorption/ionization high-energy collision-induced dissociation of steroids: analysis of oxysterols in rat brain. *Anal Chem*. 2006;**78**(1):164–173.
34. Khan MA, Wang Y, Heidelberger S, Alvelius G, Liu S, Sjövall J, Griffiths WJ. Analysis of derivatised steroids by matrix-assisted laser desorption/ionisation and post-source decay mass spectrometry. *Steroids*. 2006;**71**(1):42–53.
35. Edwards JL, Kennedy RT. Metabolomic analysis of eukaryotic tissue and prokaryotes using negative mode MALDI time-of-flight mass spectrometry. *Anal Chem*. 2005;**77**(7):2201–2209.
36. Shroff R, Muck A, Svatos A. Analysis of low molecular weight acids by negative mode matrix-assisted laser desorption/ionization time-of-flight mass spectrometry. *Rapid Commun Mass Spectrom*. 2007; **21**(20):3295–3300.
37. Miura D, Fujimura Y, Tachibana H, Wariishi H. Highly sensitive matrix-assisted laser desorption ionization-mass spectrometry for high-throughput metabolic profiling. *Anal Chem*. 2010;**82**(2): 498–504.
38. Miura D, Fujimura Y, Yamato M, Hyodo F, Utsumi H, Tachibana H, Wariishi H. Ultrahighly sensitive in situ metabolomic imaging for visualizing spatiotemporal metabolic behaviors. *Anal Chem*. 2010;**82**(23):9789–9796.
39. Sun N, Ly A, Meding S, Witting M, Hauck SM, Ueffing M, Schmitt-Kopplin P, Aichler M, Walch A. High-resolution metabolite imaging of light and dark treated retina using MALDI-FTICR mass spectrometry. *Proteomics*. 2014;**14**(7-8):913–923.
40. Gomez-Sanchez CE, Qi X, Velarde-Miranda C, Plonczynski MW, Parker CR, Rainey W, Satoh F, Maekawa T, Nakamura Y, Sasano H, Gomez-Sanchez EP. Development of monoclonal antibodies against human CYP11B1 and CYP11B2. *Mol Cell Endocrinol*. 2014;**383**(1-2):111–117.
41. Buck A, Ly A, Balluff B, Sun N, Gorzolka K, Feuchtinger A, Janssen KP, Kuppen PJ, van de Velde CJ, Weirich G, Erlmeier F, Langer R, Aubele M, Zitzelsberger H, Aichler M, Walch A. High-resolution MALDI-FT-ICR MS imaging for the analysis of metabolites from formalin-fixed, paraffin-embedded clinical tissue samples. *J Pathol*. 2015;**237**(1):123–132.
42. Xia J, Wishart DS. MetPA: a web-based metabolomics tool for pathway analysis and visualization. *Bioinformatics*. 2010;**26**(18): 2342–2344.
43. Alexandrov T, Becker M, Deininger SO, Ernst G, Wehder L, Grasmair M, von Eggeling F, Thiele H, Maass P. Spatial segmentation of imaging mass spectrometry data with edge-preserving image denoising and clustering. *J Proteome Res*. 2010;**9**(12):6535–6546.
44. Alexandrov T, Becker M, Guntinas-Lichius O, Ernst G, von Eggeling F. MALDI-imaging segmentation is a powerful tool for spatial functional proteomic analysis of human larynx carcinoma. *J Cancer Res Clin Oncol*. 2013;**139**(1):85–95.
45. Aichler M, Borgmann D, Krumsiek J, Buck A, MacDonald PE, Fox JEM, Lyon J, Light PE, Keipert S, Jastroch M, Feuchtinger A,

Mueller NS, Sun N, Palmer A, Alexandrov T, Hrabe de Angelis M, Neschen S, Tschop MH, Walch A. N-acyl taurines and acylcarnitines cause an imbalance in insulin synthesis and secretion provoking beta cell dysfunction in type 2 diabetes. *Cell Metab*. 2017; **25**(6):1334–1347.

46. Wishart DS, Tzur D, Knox C, Eisner R, Guo AC, Young N, Cheng D, Jewell K, Arndt D, Sawhney S, Fung C, Nikolai L, Lewis M, Coutouly MA, Forsythe I, Tang P, Shrivastava S, Jeroncic K, Stothard P, Amegbey G, Block D, Hau DD, Wagner J, Miniaci J, Clements M, Gebremedhin M, Guo N, Zhang Y, Duggan GE, Macinnis GD, Weljie AM, Dowlatabadi R, Bamforth F, Clive D, Greiner R, Li L, Marrie T, Sykes BD, Vogel HJ, Querengesser L. HMDB: the Human Metabolome Database. *Nucleic Acids Res*. 2007;**35**(Database issue):D521–D526.
47. Palmer A, Phapale P, Chernyavsky I, Lavigne R, Fay D, Tarasov A, Kovalev V, Fuchser J, Nikolenko S, Pineau C, Becker M, Alexandrov T. FDR-controlled metabolite annotation for high-resolution imaging mass spectrometry. *Nat Methods*. 2017;**14**(1):57–60.
48. Rege J, Karashima S, Lerario AM, Smith JM, Auchus RJ, Kasa-Vubu JZ, Sasano H, Nakamura Y, White PC, Rainey WE. Age-dependent Increases in adrenal cytochrome b5 and serum 5-androstenediol-3-sulfate. *J Clin Endocrinol Metab*. 2016;**101**(12):4585–4593.
49. Freel EM, Stanson AW, Thompson GB, Grant CS, Farley DR, Richards ML, Young WF Jr. Adrenal venous sampling for catecholamines: a normal value study. *J Clin Endocrinol Metab*. 2010; **95**(3):1328–1332.
50. Deininger SO, Ebert MP, Fütterer A, Gerhard M, Röcken C. MALDI imaging combined with hierarchical clustering as a new tool for the interpretation of complex human cancers. *J Proteome Res*. 2008;**7**(12):5230–5236.
51. McCombie G, Staab D, Stoeckli M, Knochenmuss R. Spatial and spectral correlations in MALDI mass spectrometry images by clustering and multivariate analysis. *Anal Chem*. 2005;**77**(19): 6118–6124.
52. Alexandrov T, Meding S, Trede D, Kobarg JH, Balluff B, Walch A, Thiele H, Maass P. Super-resolution segmentation of imaging mass spectrometry data: Solving the issue of low lateral resolution. *J Proteomics*. 2011;**75**(1):237–245.
53. Balluff B, Frese CK, Maier SK, Schöne C, Kuster B, Schmitt M, Aubele M, Höfler H, Deelder AM, Heck A Jr, Hogendoorn PC, Morreau J, Maarten Altelaar AF, Walch A, McDonnell LA. De novo discovery of phenotypic intratumour heterogeneity using imaging mass spectrometry. *J Pathol*. 2015;**235**(1):3–13.
54. Abdelmoula WM, Balluff B, Englert S, Dijkstra J, Reinders MJT, Walch A, McDonnell LA, Lelieveldt BPF. Data-driven identification of prognostic tumor subpopulations using spatially mapped t-SNE of mass spectrometry imaging data. *Proc Natl Acad Sci USA*. 2016;**113**(43):12244–12249.
55. Ly A, Buck A, Balluff B, Sun N, Gorzolka K, Feuchtinger A, Janssen KP, Kuppen PJ, van de Velde CJ, Weirich G, Erlmeier F, Langer R, Aubele M, Zitzelsberger H, McDonnell L, Aichler M, Walch A. High-mass-resolution MALDI mass spectrometry imaging of metabolites from formalin-fixed paraffin-embedded tissue. *Nat Protoc*. 2016;**11**(8):1428–1443.
56. Nussey S, Endocrinology SW. *An Integrated Approach*. Oxford: BIOS Scientific Publishers; 2001:115–168.
57. Kopf PG, Zhang DX, Gauthier KM, Nithipatikom K, Yi XY, Falck JR, Campbell WB. Adrenic acid metabolites as endogenous endothelium-derived and zona glomerulosa-derived hyperpolarizing factors. *Hypertension*. 2010;**55**(2):547–554.
58. Yi XY, Gauthier KM, Cui L, Nithipatikom K, Falck JR, Campbell WB. Metabolism of adrenic acid to vasodilatory 1alpha,1beta-dihomo-epoxyeicosatrienoic acids by bovine coronary arteries. *Am J Physiol Heart Circ Physiol*. 2007;**292**(5):H2265–H2274.
59. Nussdorfer G, Mazzocchi G, Rebonato L. Long-term trophic effect of ACTH on rat adrenocortical cells. An ultrastructural, morphometric and autoradiographic study. *Z Zellforsch Mikrosk Anat*. 1971;**115**(1):30–45.
60. Shelton JH, Jones AL. The fine structure of the mouse adrenal cortex and the ultrastructural changes in the zona glomerulosa with low and high sodium diets. *Anat Rec*. 1971;**170**(2):147–181.
61. Fujita H. On the fine structure of alteration of the adrenal cortex in hypophysectomized rats. *Z Zellforsch Mikrosk Anat*. 1972;**125**(4): 480–496.
62. Armato U, Nussdorfer GG, Andreis PG, Mazzochi G, Draghi E. Primary tissue culture of human adult adrencortical cells. Methodology and electron microscopic observations on ACTH-deprived and ACTH-treated cortical cells. *Cell Tissue Res*. 1974;**155**(2):155–180.
63. Merlevede W, Defreyn G, Goris J, Kalala LR, Roosemont J. Regulation of glycogen phosphorylase phosphatase activity by ATP-Mg2+ and cyclic AMP. *Arch Int Physiol Biochim*. 1976;**84**(2): 359–378.
64. Ueberberg H, Iro H, Hankwitz R, Trieb G. Investigations on the regulation of the glycogen content in the rat adrenal cortex. *Exp Pathol*. 1982;**22**(4):231–235.
65. Haase M, Willenberg HS, Bornstein SR. Update on the corticomedullary interaction in the adrenal gland. *Endocr Dev*. 2011;**20**: 28–37.
66. Patak P, Willenberg HS, Bornstein SR. Vitamin C is an important cofactor for both adrenal cortex and adrenal medulla. *Endocr Res*. 2004;**30**(4):871–875.
67. Kanczkowski W, Sue M, Bornstein SR. Adrenal gland microenvironment and its involvement in the regulation of stress-induced hormone secretion during sepsis. *Front Endocrinol (Lausanne)*. 2016;**7**:156.
68. Weiss ID, Huff LM, Evbuomwan MO, Xu X, Dang HD, Velez DS, Singh SP, Zhang HH, Gardina PJ, Lee JH, Lindenberg L, Myers TG, Paik CH, Schrump DS, Pittaluga S, Choyke PL, Fojo T, Farber JM. Screening of cancer tissue arrays identifies CXCR4 on adrenocortical carcinoma: correlates with expression and quantification on metastases using 64Cu-plerixafor PET. *Oncotarget*. 2017;**8**(43): 73387–73406.
69. Bluemel C, Hahner S, Heinze B, Fassnacht M, Kroiss M, Bley TA, Wester HJ, Kropf S, Lapa C, Schirbel A, Buck AK, Herrmann K. Investigating the chemokine receptor 4 as potential theranostic target in adrenocortical cancer patients. *Clin Nucl Med*. 2017; **42**(1):e29–e34.
70. Kanczkowski W, Alexaki VI, Tran N, Großklaus S, Zacharowski K, Martinez A, Popovics P, Block NL, Chavakis T, Schally AV, Bornstein SR. Hypothalamo-pituitary and immune-dependent adrenal regulation during systemic inflammation. *Proc Natl Acad Sci USA*. 2013;**110**(36):14801–14806.